# Investigation of the Antibacterial Activity and Underlying Mechanism of Terminalia chebula Retz. Against Helicobacter pylori

**Yangchenze Fan**
Baotou Medical College, Inner Mongolia University of Science and Technology，Baotou
**Xuanru Kang**
Baotou Medical College, Inner Mongolia University of Science and Technology，Baotou
**Xianmei Meng**
Baotou Medical College, Inner Mongolia University of Science and Technology，Baotou
**Zhenyu Jiang**
Baotou Medical College, Inner Mongolia University of Science and Technology，Baotou
**Chi Wang**
Baotou Medical College, Inner Mongolia University of Science and Technology，Baotou
**Jiaying Zhu**
Baotou Medical College, Inner Mongolia University of Science and Technology，Baotou
**Yuanyuan Nian**
nianyuanyuannina@163.com

Baotou Medical College, Inner Mongolia University of Science and Technology，Baotou

**Research Article**

**Keywords:** Terminalia chebula Retz., Helicobacter pylori, network pharmacology, ABL1, PTPN11, c-k-Ras, ellagic acid, signaling pathway, anti-inflammatory effect

**Posted Date:** February 11th, 2026

**DOI:** https://doi.org/10.21203/rs.3.rs-8635950/v1



**Additional Declarations:** No competing interests reported.

## Abstract

**Objective** To investigate the antibacterial activity and underlying mechanism of Terminalia chebula Retz. against Helicobacter pylori (H. pylori).

**Methods** Core targets of T. chebula for inhibiting H. pylori were obtained via network pharmacology, followed by enrichment analysis. Molecular docking was performed to verify the binding activity between the active components of T. chebula and the core targets. A rat model of H. pylori infection was established, and the rats were randomly divided into the blank control group, model control group, and high-, medium-, and low-dose T. chebula groups. Routine blood test results of each group were examined, and the H. pylori infection status, the contents of interleukin-12 (IL-12), interleukin-17 (IL-17), interleukin-23 (IL-23), interferon-γ (IFN-γ), tumor necrosis factor-α (TNF-α) in gastric mucosa, as well as the protein expression levels of related targets ABL1, PTPN11, and Ras were determined. Minimum inhibitory concentration (MIC) and minimum bactericidal concentration (MBC) tests were conducted using the Hp SS1 strain.

**Results** Network pharmacology identified 11 key targets of T. chebula for H. pylori inhibition. Enrichment analysis indicated that the inhibitory mechanism of T. chebula against H. pylori may be associated with the RAS signaling pathway, signal transduction pathways and functions of the Eph receptor family and its ligands, and cancer pathways. Molecular docking results showed that the main active components, including ellagic acid, quinidine sulfate, and sennosides, exhibited high docking affinity with the core targets ABL1, PTPN11, and PARP1. Animal experiments revealed obvious gastric mucosal damage in H. pylori-infected rats. After treatment with medium and high doses of T. chebula, the number of inflammatory cells in the gastric mucosa of rats significantly decreased, swelling was alleviated, and mucosal thickness returned to normal. Meanwhile, the serum levels of TNF-α, IL-12, IL-17, IL-23, and IFN-γ were reduced ($P < 0.05$), and the protein expression levels of ABL1, PTPN11, and Ras were downregulated ($P < 0.05$), with the most significant reduction and the best anti-inflammatory effect observed in the high-dose T. chebula group. Routine blood test results demonstrated that T. chebula treatment significantly decreased the white blood cell count ($P < 0.05$). Drug sensitivity tests showed that quinidine sulfate, ellagic acid, sennosides, (R)-(6-methoxy-4-quinolyl)-[(2R,4R,5S)-5-vinylquinuclidin-2-yl]methanol, and Sennoside E_qt exerted significant in vitro antibacterial activity.

**Conclusion** Terminalia chebula exerts a therapeutic effect on H. pylori infection by acting on targets such as ABL1, PTPN11, and c-k-Ras through components including ellagic acid, quinidine sulfate, and sennosides. It inhibits related pathways to downregulate the expression of various cytokines, thereby alleviating gastric mucosal inflammatory damage.

## Introduction

The global infection rate of Helicobacter pylori (H. pylori) exceeds 50%. H. pylori is the primary cause of chronic gastritis and peptic ulcers, and also the most important modifiable risk factor for gastric cancer. However, current mainstream therapies exhibit significant side effects, and drug resistance has become a prominent issue, highlighting an urgent need to develop safer and more effective novel drugs or vaccines.

Terminalia chebula Retz., the mature fruit of a plant belonging to the genus Terminalia in the family Combretaceae, is a highly representative research object in traditional medical systems and the history of cross-cultural exchanges. Numerous studies have confirmed its excellent antibacterial activity [17, 18]. Our research team has previously conducted relevant explorations; drug sensitivity tests on 13 commonly used single Chinese-Mongolian medicines showed that T. chebula has good antibacterial activity against the standard H. pylori strain (ATCC43504) [5]. Nevertheless, the antibacterial mechanism of T. chebula against H. pylori remains unclear and requires further in-depth investigation.

This study intends to utilize the characteristics of network pharmacology—including integrity, systematicness, and consistency with the multi-component and multi-target properties of traditional Chinese medicines—to predict the targets and pathways underlying the antibacterial effect of T. chebula against H. pylori. Molecular docking and animal experiments will be combined to verify the reliability of the results, thereby providing a reference for the in-depth clinical research and development of T. chebula.

## Materials and Methods

# 1.1 Network Pharmacology Analysis of Terminalia chebula Retz. and Helicobacter pylori

# 1.1.1 Collection of Active Components and Targets of Terminalia chebula Retz.

"HE ZI" was used as the search term to screen for active components. The Traditional Chinese Medicine Systems Pharmacology Database (TCMSP, https://old.tcmsp-e.com/tcmsp.php) was queried to obtain active components of T. chebula that met the criteria of oral bioavailability (OB) ≥ 30% and drug-likeness (DL) ≥ 0.18. The structural files of these active components were then imported into the PharmMapper database (http://www.lilab-ecust.cn/pharmmapper/) to acquire their corresponding targets.

# 1.1.2 Construction of the "Active Component-Target" Network

The active components and their targets of T. chebula obtained in Section 1.1.1 were imported into Cytoscape software to construct the "Active Component-Target" network.

## 1.1.3 Collection of Helicobacter pylori-Related Targets

GeneCards database (https://www.genecards.org/) was searched with the keywords "H. pylori" and "inflammation" to collect target information related to H. pylori-induced diseases. The targets of T. chebula active components and the pathogenic targets of H. pylori were intersected using the online tool Venny 2.1.0 (http://www.liuxiaoyuyuan.cn/) to obtain the common genes associated with both T. chebula and H. pylori.

## 1.1.4 Construction of Protein-Protein Interaction (PPI) Network

The intersection target genes obtained in Section 1.1.3 were imported into the String database, with "Homo sapiens" set as the species and the interaction score threshold set at 0.15, to generate the PPI network.

## 1.1.5 GO and KEGG Pathway Enrichment Analyses

The key targets obtained in Section 1.1.4 were imported into the DAVID database (https://david.ncifcrf.gov/). "Official Gene Symbol" and "Gene List" were clicked sequentially, and "Homo sapiens" was selected as the species. After uploading the data, KEGG pathway enrichment analysis was performed, and Gene Ontology (GO) analysis was conducted from three aspects: biological process (BP), cellular component (CC), and molecular function (MF). A P-value < 0.05 indicated statistically significant differences. The data were exported to Excel for processing and then imported into the Bioinformatics website (http://www.bioinformatics.com.cn/) to generate bar charts for GO analysis and bubble charts for KEGG pathway analysis.

## 1.1.6 Molecular Docking Verification

The top-ranked targets in the PPI network (based on degree value) were used as receptors, and the top-ranked active components of T. chebula in the "Active Component-Target" network were used as ligands to predict their binding ability. A lower binding energy value indicated a stronger binding ability. The gene names of key target proteins were entered into the UniProt database (https://www.uniprot.org/) to retrieve their UniProt IDs. These UniProt IDs were then input into the RCSB PDB database (https://www.rcsb.org/) to find the corresponding target proteins, whose 3D structures were downloaded and saved in PDB format. The structures were imported into PyMOL software for dehydration and ligand removal, followed by hydrogenation using AutoDock software and export in PDBQT format. The mol2 structures of T. chebula active components were downloaded from TCMSP, imported into ChemBio3D Ultra 14.0 for energy minimization (with the Minimum RMS Gradient set to 0.001), and saved in mol2 format. The optimized small molecules were imported into AutoDockTools-1.5.6 for hydrogenation, charge calculation, charge assignment, and rotatable bond setting, then saved in PDBQT format. The proteins were imported into PyMOL 2.3.0 to remove crystal water and original ligands, then imported into AutoDockTools (v1.5.6) for hydrogenation, charge calculation, charge assignment, and atom type specification, followed by saving in PDBQT format. POCASA 1.1 was used to predict protein binding sites, and AutoDock Vina 1.1.2 was employed for docking. PyMOL 2.3.0 was utilized to analyze the interaction modes of the docking results.

## 1.2 Animal Model Validation

## 1.2.1 Animals and Strains

Forty specific pathogen-free (SPF) male Sprague-Dawley (SD) rats, weighing 170–190 g, were purchased from Beijing Vital River Laboratory Animal Technology Co., Ltd. (License No.: SCXK (Jing) 2024-0001). All rats were subjected to a 7-day acclimatized feeding period. This study was approved by the Ethics Committee of Baotou Medical College, Inner Mongolia University of Science and Technology. Helicobacter pylori (H. pylori) SS1 strain was purchased from Hangzhou Hongsai Biotechnology Co., Ltd. and stored at -80℃. Reagents used included BHI medium (HB8478, Qingdao Haibo Biotechnology Co., Ltd.), defibrinated sheep blood (1001339-1, Qingdao Haibo Biotechnology Co., Ltd.), and agar (A1296, Sigma).

## 1.2.2 Drugs

Forty grams of Terminalia chebula Retz. powder, prepared by the Traditional Chinese Medicine Pharmacy of the Second Affiliated Hospital of Baotou Medical College, Inner Mongolia University of Science and Technology, was made into a water decoction by conventional decoction method and stored at 4℃ under refrigeration.

## 1.2.3 Main Reagents

HE staining kit (Batch No.: BT-P107), rabbit monoclonal antibody against c-Abl (260 kDa, Batch No.: A22082), rabbit polyclonal antibodies against PTPN11 (68 kDa, Batch No.: 20145-1-AP) and c-k-Ras (21 kDa, Batch No.: 12063-1-AP), rat TNF-α, IL-12, IL-17, IL-23, and IFN-γ ELISA kits (Batch Nos.: ER1393, ER1086, ER0035, ER1096, ER0012 respectively), and 0.22 μm NC membrane (PALL, Cat. No.: P-N66485-30).

## 1.2.4 Animal Modeling, Administration, and Grouping

Rats were intragastrically administered 2.5% amoxicillin solution (0.5 ml per time, twice a day) for 3 consecutive days to eliminate miscellaneous bacteria in the digestive tract. After a 2-day rest, modeling was performed via intragastric gavage. All rats were fasted for 12 hours with free access to water before modeling. Pretreatment drugs, including 0.1 mmol/L $NaHCO_3$ solution, 56% ethanol, 5 mg/ml indomethacin solution, and 2 g/L $NaHCO_3$ + indomethacin solution, were intragastrically administered at 0.5 ml per rat. Fasting with free access to water was continued, and 6 hours later, H. pylori bacterial solution (1.5 ml per rat, concentration of $10^9$ CFU/ml) was given by gavage. All rats were fasted and deprived of water for 4 hours after H. pylori gavage, followed by normal feeding. Rats were gavaged every other day for a total of 5 times with H. pylori bacterial solution. Two rats were

randomly sacrificed after the last gavage, and gastric antrum mucosa was collected for Gram staining and rapid urease test. Double positive results were considered as successful H. pylori colonization.

Model rats were randomly divided into the model control group, low-dose, medium-dose, and high-dose T. chebula groups, with 6 rats in each group (8 rats died during modeling due to individual factors and feeding conditions). Administration was initiated on the 2nd day after modeling. Rats in the low-, medium-, and high-dose T. chebula groups were given T. chebula aqueous extract at 30, 60, and 90 mg/kg respectively (dose design was based on published literature [1]). Rats in the blank control group and model control group were given an equal volume of normal saline by gavage. All rats were gavaged every other day for 4 consecutive weeks.

### 1.2.5 Detection of Whole Blood Indicators in Rats

After the end of administration, whole blood of rats in each group was collected into EDTA-K2 anticoagulant tubes and detected using a Mindray veterinary automatic hematology analyzer (Model: BC-5000vet). Changes in the counts of white blood cells, red blood cells, neutrophils, lymphocytes, and other indicators were recorded.

### 1.2.6 HE Staining

Paraffin sectioning and HE staining: Tissues were fixed with 4% paraformaldehyde, subjected to gradient ethanol dehydration, and embedded in paraffin. Then 5 μm-thick sections were cut, and pathological morphology was observed after HE staining.

### 1.2.7 ELISA Detection of Serum TNF-α, IL-12, IL-17, IL-23, and IFN-γ Levels

Blood was collected from the orbital venous plexus, centrifuged to collect the upper serum, and the contents of TNF-α, IL-12, IL-17, IL-23, and IFN-γ in rat serum were detected in accordance with the ELISA kit instructions.

### 1.2.8 Western Blot Analysis of c-Abl, PTPN11, and c-k-Ras Protein Levels

Total protein was extracted from rat gastric tissues using RIPA lysis buffer, and protein quantification was performed with a BCA protein assay kit. Then 40 μg of protein was separated by 15% SDS-PAGE gel electrophoresis and transferred to a PVDF membrane. The membrane was incubated overnight at 4℃ with primary antibodies against GAPDH (1:50000), c-Abl (1:3000), PTPN11 (1:5000), and c-k-Ras (1:5000). After membrane washing, HRP-labeled secondary antibodies (goat anti-rabbit, 1:1000; goat anti-mouse, 1:10000) were added, and the PVDF membrane was soaked in the secondary antibody incubation solution and incubated on a shaker at room temperature for 2 hours.

## 1.3 In Vitro Antibacterial Assay of Active Components from Terminalia chebula Retz. Against H. pylori

Drug stock solutions were prepared for Sennoside E_qt, ellagic acid, and quinidine sulfate.

((R)-(6-methoxy-4-quinolyl)-[(2R,4R,5S)-5-vinylquinuclidin-2-yl]methanol). BHI solid medium supplemented with defibrinated sheep blood was prepared as follows: 26 g of BHI powder and 7.5 g of agar dissolved in 500 mL of distilled water, autoclaved at 121°C for 15 min, and supplemented with 5% defibrinated sheep blood prior to use. Drug-containing medium was prepared via serial dilution (in 24-well plates, with the 8th well as the control). NC membranes were placed into each well. H. pylori was verified by 16S rRNA sequencing, adjusted to an $OD_{600}$ value of 0.3, and then diluted 1000-fold. A 20 μL aliquot of the diluted bacterial suspension was spotted onto the NC membranes, followed by incubation under microaerophilic conditions at 37°C for 7 days. The minimum inhibitory concentration (MIC) was defined as the lowest concentration at which no visible colonies grew on the NC membranes. For the determination of the minimum bactericidal concentration (MBC), bacterial cultures were incubated at a concentration equal to the MIC; the MBC was defined as the lowest concentration yielding fewer than 10 colonies.

## 1.4 Statistical Analysis

Statistical analyses were performed using SPSS 26.0 software, and graphs were plotted with GraphPad Prism 8.0.2 software (note: corrected the typo “Priam” to the standard software name “Prism”). Measurement data were expressed as mean ± standard deviation ($\bar{x} \pm s$). One-way analysis of variance (ANOVA) was used for comparisons among multiple groups with a single factor, and pairwise comparisons between groups were conducted using the least significant difference (LSD) test. A P-value < 0.05 was considered statistically significant.

# Results

## 2.1 Results of Network Pharmacology Analysis of Terminalia chebula Retz. and Helicobacter pylori

### 2.1.1 Active Components of Terminalia chebula Retz. and Their Corresponding Targets

A total of 8 active components were obtained from the TCMSP database, namely Sennoside E_qt, ellagic acid, 7-Dehydrosigmasterol, chebulic acid, Ellipticine, (R)-(6-methoxy-4-quinolyl)-[(2R,4R,5S)-5-vinylquinuclidin-2-yl]methanol, Peraksine, and Cheilanthifoline, corresponding to a total of 421

targets. Detailed information is presented in Table 1.

Table 1
Active Components and Corresponding Targets of Terminalia chebula Retz.

| No. | Name | Molecular Formula | Number of Targets |
|---|---|---|---|
| 1 | ellagic acid | $C_{14}H_6O_8$ | 291 |
| 2 | Sennoside E_qt | $C_{42}H_{38}O_{20}$ | 290 |
| 3 | 7-Dehydrosigmasterol | $C_{29}H_{50}O$ | 213 |
| 4 | chebulic acid | $C_{14}H_{12}O_{11}$ | 290 |
| 5 | Ellipticine | $C_{17}H_{14}N_2$ | 185 |
| 6 | (R)-(6-methoxy−4-quinolyl)-[(2R,4R,5S)−5-vinylquinuclidin−2-yl]methanol | $C_{20}H_{24}N_2O_2$ | 278 |
| 7 | Peraksine | $C_{19}H_{22}N_2O_2$ | 236 |
| 8 | Cheilanthifoline | $C_{19}H_{19}NO_4$ | 246 |

## 2.1.2 Construction of the "Active Component-Target-Disease" Network

The "Active Component-Target" diagram is shown in Fig. 1. The relevant data were imported into Cytoscape software to visualize the targets of the active components of Terminalia chebula Retz. and the pathogenic targets of Helicobacter pylori.

## 2.1.3 Collection of H. pylori Targets and Acquisition of Drug-Disease Targets

A total of 99 pathogenic targets of Helicobacter pylori were identified via screening with the GeneCards database. Finally, 11 potential therapeutic targets of Terminalia chebula Retz. against H. pylori were obtained using the Venn database 2.1.0, with detailed information presented in Fig. 2.

## 2.1.4 Construction of Protein-Protein Interaction (PPI) Network

The obtained intersection target genes were imported into the String database. The resulting data were visualized using Cytoscape 3.8.0 software, and the protein-protein interaction network as well as the core target network were plotted, as shown in Fig. 3. The PPI network contained 11 nodes, and several key genes including ABL1, PTPN11, and PARP1 were identified via screening.

## 2.1.5 GO and KEGG Pathway Enrichment Analysis

GO functional enrichment analysis and KEGG pathway analysis were performed on the 11 key targets obtained in Section 2.1.4 using the DAVID 6.8 database. GO analysis was conducted from three aspects, namely Biological Process (BP), Cellular Component (CC), and Molecular Function (MF), yielding a total of 60 GO analysis results. Bar charts of GO analysis were plotted according to the P-value, as shown in Figs. 4, 5, and 6; the taller the bar, the greater the number of genes involved in the corresponding process. Among these results, 47 GO terms had a P-value < 0.05. The BP-related terms included signal transduction pathways and functions of the Eph receptor family and its ligands, positive regulation of peptidyl-tyrosine phosphorylation, negative regulation of the apoptotic process, glutathione derivative biosynthesis, and cellular response to lipopolysaccharide. The CC-related terms included ficolin-1-rich granule lumen, mitochondrion, macromolecular complex, extracellular space, and extracellular region. The MF-related terms included serine-type endopeptidase activity, protein binding, glutathione transferase activity, enzyme binding, and phosphotyrosine binding. A total of 15 KEGG pathways were identified, and bubble charts of KEGG pathway analysis were plotted according to the P-value; the darker the bubble color, the higher the correlation between the pathway and the disease, as shown in Fig. 7. Among these pathways, 7 had a P-value < 0.05, namely chemical carcinogenesis-reactive oxygen species, Ras signaling pathway, cancer pathways, atherosclerosis, hepatocellular carcinoma, axon guidance, and proteoglycans in cancer. The main involved targets included ABL1, GSTM1, and PTPN11.

## 2.1.6 Molecular Docking Verification

In this study, the binding affinities between the top-ranked targets (ABL1, PARP1, and PTPN11) in the PPI network and the active components (ellagic acid, quinidine sulfate, and Sennoside E_qt) were predicted, with the target proteins serving as receptors and the active components as ligands. Generally, it is recognized that the more stable the binding conformation between the receptor and ligand, the lower the binding energy and the stronger the interaction. According to the docking results, the binding energies between all components and targets were negative, indicating that these components and targets exhibited favorable binding activities. Ellagic acid, quinidine sulfate, and Sennoside E_qt showed relatively low binding energies with ABL1, PARP1, and PTPN11, suggesting good binding capabilities. All the docking binding energy results are presented in Table 2. The molecular docking diagrams are shown in Fig. 8.

Table 2
Molecular Docking Binding Energies

| Component | Target | Binding Energy (kcal/mol) |
|---|---|---|
| ellagic acid | ABL1 | −7.5 |
| ellagic acid | PARP1 | −9.4 |
| ellagic acid | PTPN11 | −8.2 |
| quinidine sulfate | ABL1 | −7.5 |
| quinidine sulfate | PARP1 | −8.6 |
| quinidine sulfate | PTPN11 | −7.3 |
| Sennoside E_qt | ABL1 | −9 |
| Sennoside E_qt | PARP1 | −8.4 |
| Sennoside E_qt | PTPN11 | −8 |

## 2.2 Animal Experiment Results

### 2.2.1 Routine Blood Test Results

Analysis of routine blood test indicators showed that statistical analyses were performed on the differences in multiple blood parameters among different treatment groups, including the Normal Group, Model Group, Terminalia chebula Low-Dose Group, Terminalia chebula Medium-Dose Group, and Terminalia chebula High-Dose Group. The results indicated that compared with the Normal Group, the white blood cell (WBC) counts in the Model Group, as well as the low-, medium-, and high-dose groups of Terminalia chebula, were significantly increased ($P < 0.05$). In contrast, compared with the Model Group, the WBC counts in the low-, medium-, and high-dose groups of Terminalia chebula were significantly decreased ($P < 0.05$). Additionally, there were differences in some indicators among the low-, medium-, and high-dose groups of Terminalia chebula. Details are shown in Table 3.

Table 3
Routine Blood Test Results

| Variable Name | Normal | Model 1 | Terminalia chebula Retz.-Low-Dose* | Terminalia chebula Retz.-Medium-Dose* | Terminalia chebula Retz.-High-Dose* | F/Z | P Value |
|---|---|---|---|---|---|---|---|
| White Blood Cell (WBC) Count | 2.44 ± 0.36 | 2.41 ± 0.03a | 2.44 ± 0.36abc | 4.07 ± 0.08abc | 3.3 ± 0.08bcd | 439.462[1]) | 0.001 |
| Neutrophil Count | 0.4 ± 0.2 | 0.18 ± 0 | 0.4 ± 0.2 | 0.48 ± 0.03 | 0.46 ± 0.02 | 11.153(2) | 0.025 |
| Lymphocyte Count | 1.74 ± 0.56 | 1.98 ± 0.01 | 1.74 ± 0.56 | 2.99 ± 0.01b | 1.95 ± 0.07 | 11.142[2]) | 0.025 |
| Monocyte Count | 0.28 ± 0.16 | 0.25 ± 0.03 | 0.28 ± 0.16 | 0.57 ± 0.1b | 0.85 ± 0.13 | 11.265[2]) | 0.024 |
| Eosinophil Count | 0.01 ± 0.02 | 0.01 ± 0.01 | 0.01 ± 0.02 | 0.03 ± 0.01 | 0.04 ± 0.01 | 5.409[2]) | 0.248 |
| Basophil Count | 0 ± 0.01 | 0 ± 0 | 0 ± 0.01 | 0 ± 0 | 0 ± 0.01 | 5.327[2]) | 0.255 |
| Neutrophil Percentage | 16.63 ± 9.61 | 7.53 ± 0.12 | 16.63 ± 9.61 | 11.73 ± 1.01 | 13.73 ± 0.38 | 8.181[2]) | 0.085 |
| Lymphocyte Percentage | 70.67 ± 17.08 | 81.7 ± 0.87 | 70.67 ± 17.08 | 73.50 ± 1.39 | 59.07 ± 3.76 | 7.747[2]) | 0.101 |
| Monocyte Percentage | 11.97 ± 8.08 | 10.3 ± 1.13 | 11.97 ± 8.08 | 13.93 ± 2.15 | 25.77 ± 3.46 | 5.844[2]) | 0.211 |
| Eosinophil Percentage | 0.53 ± 0.76 | 0.4 ± 0.3 | 0.53 ± 0.76 | 0.83 ± 0.21 | 1.23 ± 0.4 | 8.763[2]) | 0.067 |
| Eosinophil Percentage | 0.2 ± 0.1 | 0.07 ± 0.12 | 0.2 ± 0.1 | 0 ± 0 | 0.2 ± 0.17 | 8.636[2]) | 0.071 |
| Red Blood Cell (RBC) Count | 6.64 ± 0.69 | 7.66 ± 0.13 | 6.64 ± 0.69 | 8.6 ± 0.22 | 8.73 ± 0.16 | 11.233[2]) | 0.024 |
| Hemoglobin (HGB) | 144 ± 11.53 | 156.33 ± 0.58 | 144 ± 11.53 | 168 ± 1.00b | 169.67 ± 0.58 | 11.457[2]) | 0.022 |
| Hematocrit (HCT) | 42.63 ± 3.5 | 46.27 ± 0.74 | 42.63 ± 3.5 | 49.4 ± 1.15 | 50.23 ± 0.75 | 9.851[2]) | 0.043 |
| Mean Corpuscular Volume (MCV) | 64.4 ± 3.75 | 60.43 ± 0.06 | 64.4 ± 3.75 | 57.43 ± 0.12 | 57.57 ± 0.21 | 7.702[2]) | 0.103 |
| Mean Corpuscular Hemoglobin (MCH) | 21.77 ± 1.21 | 20.43 ± 0.31 | 21.77 ± 1.21 | 19.53 ± 0.46b | 19.43 ± 0.31 | 11.855[2]) | 0.018 |
| Mean Corpuscular Hemoglobin Concentration (MCHC) | 337.67 ± 1.53 | 338.33 ± 4.04 | 337.67 ± 1.53 | 340.00 ± 6.93 | 337.67 ± 4.16 | 5.011[2]) | 0.286 |
| Red Blood Cell Distribution Width-Coefficient of Variation (RDW-CV) | 14.03 ± 0.65 | 14.7 ± 0.2 | 14.03 ± 0.65 | 13.93 ± 0.06b | 14.07 ± 0.12 | 10.841[2]) | 0.028 |
| Red Blood Cell Distribution Width-Standard Deviation (RDW-SD) | 35.43 ± 1.36 | 34.93 ± 0.35 | 35.43 ± 1.36b | 31 ± 0.17b | 32 ± 0.35 | 12.894[2]) | 0.012 |
| Platelet (PLT) Count | 768.67 ± 3.51 | 662.67 ± 10.6 | 768.67 ± 3.51 | 582.67 ± 15.89b | 643 ± 12.17 | 13.233[2]) | 0.01 |
| Mean Platelet Volume (MPV) | 6.17 ± 0.4 | 6.47 ± 0.06 | 6.17 ± 0.4 | 6.8 ± 0.1 | 6.33 ± 0.06 | 11.621[2]) | 0.02 |
| Platelet Distribution Width (PDW) | 15.37 ± 0.15 | 15.33 ± 0.12 | 15.37 ± 0.15 | 15.53 ± 0.12 | 15.6 ± 0 | 11.729[2]) | 0.019 |

Note: 1) denotes F value; 2) denotes Z value; a denotes $P < 0.05$ vs. Control Group; b denotes $P < 0.05$ vs. Model Group; c denotes $P < 0.05$ vs. Terminalia chebula Retz. Low-Dose Group; d denotes $P < 0.05$ vs. Terminalia chebula Retz. Medium-Dose Group.

## 2.2.2 Pathological Analysis of Gastric Mucosa in Rats

In this study, Hematoxylin-Eosin (HE) staining was employed to analyze the pathological changes of gastric mucosa in rats. Compared with rats in the Model Group, those in the Terminalia chebula Low-Dose Group showed clearly distinguishable structures of all layers of gastric tissue under light microscopy: the mucosal epithelial cells were regularly arranged, various cell types were abundant, mild cell detachment was observed locally, and no

significant inflammatory infiltration was found overall. For rats in the Terminalia chebula Medium-Dose and High-Dose Groups, the structures of all layers of gastric tissue were also clearly distinguishable under light microscopy, with regularly arranged mucosal epithelial cells, abundant various cell types, appropriate mucosal thickness, and no significant inflammatory infiltration overall. Among these groups, the aforementioned improvement effects were more pronounced in the High-Dose Group. However, under light microscopy, abnormalities were detected in the liver tissue of rats in all Terminalia chebula Low-Dose, Medium-Dose, and High-Dose Groups. Cytoplasmic transparency was observed in hepatocytes within a large area of hepatic parenchyma; numerous hepatocytes exhibited obscure structures with local nuclear fragmentation, and the overall tissue structure showed significant changes. These findings suggest that Terminalia chebula may have hepatotoxicity [18]. Representative images are shown in Fig. 9.

2.2.3 Effects of Different Doses of Terminalia chebula Retz. on Serum Levels of TNF-α, IL-12, IL-17, IL-23, and IFN-γ in Model Rats

Helicobacter pylori (H. pylori) infection significantly increased the concentrations of pro-inflammatory cytokines, including TNF-α, IL-12, IL-17, IL-23, and IFN-γ. After intervention with Terminalia chebula Retz., the concentrations of these pro-inflammatory cytokines were significantly reduced ($P < 0.05$) in a dose-dependent manner: the most significant reduction was observed in the High-Dose Group, followed by the Medium-Dose Group, while the effect was relatively weaker in the Low-Dose Group. Details are shown in Table 4.

Table 4
Comparison of Serum Levels of TNF-α, IL-12, IL-17, IL-23, and IFN-γ Among Different Groups of Rats

| Group | Number of Animals | TNF-a | IL12 | IL17 | IL23 | IFN-Y |
|---|---|---|---|---|---|---|
| Control Group | 6 | 153.070 ± 17.50 | 192.658 ± 32.337 | 355.422 ± 41.936 | 306.175 ± 49.566 | 270.501 ± 55.407 |
| 55Model Group | 6 | 759.954 ± 84.590▯▯▯ | 967.426 ± 108.6▯▯▯34 | 1680.499 ± 180.350▯▯▯ | 1562.661 ± 159.022▯▯▯ | 1362.990 ± 90.166▯▯▯ |
| Terminalia chebula Retz. High-Dose Group | 6 | 291.246 ± 22.806▯▯▲▲▲●●● | 359.466 ± 28.371▯▯▲▲▲●●● | 552.715 ± 46.361▯▲▲▲●●● | 552.243 ± 46.110▯▯▲▲▲●●● | 524.196 ± 28.882▯▯▯▲▲▲●●● |
| Terminalia chebula Retz. Medium-Dose Group | 6 | 431.890 ± 28.925▯▯▯▲▲▲●● | 558.660 ± 44.076▯▯▯▲▲▲●●● | 1048.366 ± 66.816▯▯▯●● | 768.972 ± 38.191▯▲▲▲●●● | 680.951 ± 28.765▯▯▯▲▲▲●●● |
| Terminalia chebula Retz. Low-Dose Group | 6 | 579.700 ± 28.925▯▯▯▲▲ | 804.164 ± 30.898▯▯▯▲▲ | 1418.140 ± 73.910▯▯▯▲▲ | 1272.884 ± 65.440▯▯▲▲ | 1182.799 ± 55.037▯▯▯▲▲ |

## 2.2.4 Effects of Terminalia chebula Retz. on the Protein Expression of c-Abl, PTPN11, and c-k-Ras

Compared with the Control Group, the protein levels of c-Abl, PTPN11, and c-k-Ras in the H. pylori Model Group were significantly elevated. In comparison with the Model Group, the protein levels of c-Abl, PTPN11, and c-k-Ras were decreased in the Medium-Dose and High-Dose Groups of Terminalia chebula Retz. ($P < 0.05$), with a more significant reduction observed in the High-Dose Group ($P < 0.01$). Western Blot (WB) band images and protein level bar charts showed that the gray value changes of protein bands in each group were consistent with the quantitative results, as shown in Figs. 10 and 11.

**Note**

CON = Control Group; Hp = H. pylori Infection Group; H-L = Terminalia chebula Retz. Low-Dose Group; H-M = Terminalia chebula Retz. Medium-Dose Group; H-H = Terminalia chebula Retz. High-Dose Group

## 2.3 Antimicrobial Susceptibility Test Results

The growth of bacterial cells was observed by visual inspection. The minimum inhibitory concentration (MIC) and minimum bactericidal concentration (MBC) of (R)-(6-methoxy-4-quinolyl)-[(2R,4R,5S)-5-vinylquinuclidin-2-yl]methanol were 0.625 mg/ml and 1.25 mg/ml, respectively; those of ellagic acid were 0.0625 mg/ml and 0.25 mg/ml, respectively; and those of Sennoside E_qt were 2.5 mg/ml and 10 mg/ml, respectively. Details are shown in Table 5.

Table 5
Antimicrobial Susceptibility Test of Terminalia chebula Retz. Active Components Against H.pylori

| Number | Molecular name | Solvent | MIC(mg/ml) | MBC(mg/ml) |
|---|---|---|---|---|
| 1 | (R)-(6-methoxy−4-quinolyl)-[(2R,4R,5S)−5-vinylquinuclidin−2-yl]methanol | DMSO | 0.625 | 1.25 |
| 2 | ellagic acid | DMSO | 0.0625 | 0.25 |
| 3 | Sennoside E gt | DMSO | 2.5 | 10 |

## Discussion

Helicobacter pylori (H. pylori) infection is globally prevalent, and the growing problem of drug resistance has made the development of novel and efficient therapeutic strategies an urgent priority. As a medicinal herb commonly used for treating gastrointestinal disorders in traditional Chinese-Mongolian medicine, Terminalia chebula Retz. has been confirmed by modern studies to possess anti-inflammatory and broad-spectrum antibacterial activities, which provides a potential basis for its anti-H. pylori research. However, current research on the anti-H. pylori effects of T. chebula is still limited to preliminary in vitro reports, and its systematic pharmacological mechanism remains unclear. To address this gap, the present study established an integrated research framework of "target prediction–molecular interaction–in vitro and in vivo validation", aiming to systematically elucidate the multi-component, multi-target, and multi-pathway synergistic mechanism underlying the anti-H. pylori activity of T. chebula, thereby providing scientific evidence for the development of new anti-H. pylori drugs based on Chinese-Mongolian medicinal herbs.

Network pharmacology approaches identified 11 core overlapping targets associated with H. pylori pathogenicity for the active components of T. chebula. KEGG pathway analysis revealed that the Ras signaling pathway serves as a core mechanism, whose role in H. pylori-induced gastritis and carcinogenesis has been well-documented [13]. This prediction was verified in our animal experiments: H. pylori infection significantly upregulated the protein expression of c-Abl1, PTPN11 (SHP2), and c-k-Ras in gastric mucosa, whereas treatment with medium and high doses of T. chebula aqueous extract significantly downregulated their expression. This is consistent with the growing recognition in the academic community that the ABL1/SHP2/Ras module acts as a key signaling node in cell growth and inflammation [14, 16, 15]. Our work is the first to directly link the anti-H. pylori activity of T. chebula to the inhibition of this specific signaling axis, which not only suggests its potential in eradicating the bacterium but also implies its possible role in blocking the progression of precancerous lesions. Furthermore, the improvement of hematological parameters (including the normalization of white blood cell counts) and antimicrobial susceptibility tests further confirmed the systemic anti-inflammatory effects of T. chebula, in contrast to traditional therapies that may overlook hematological indicators. Meanwhile, the integration of network pharmacology into the present study has provided a more in-depth mechanistic interpretation.

Furthermore, the significant reduction in the levels of key pro-inflammatory cytokines (TNF-α, IL-12, IL-17, IL-23, and IFN-γ) in the serum of rats from the T. chebula treatment groups provides compelling evidence for its potent anti-inflammatory activity. The excessive production of these cytokines, particularly IL-17 and TNF-α, is a hallmark of H. pylori-associated inflammation and contributes to tissue damage [4]. The dose-dependent inhibitory effect of T. chebula on these cytokines is consistent with the findings of Ou et al. [10], who demonstrated that the aqueous extract of T. chebula can inhibit H. pylori-induced inflammatory responses by modulating inflammasome signaling pathways. Our findings extend this understanding by linking cytokine inhibition to the downregulation of upstream signaling proteins such as PTPN11/SHP2. The role of SHP2 in inflammation is complex; for instance, Imai S et al. [2] demonstrated that the oncogenic phosphatase SHP2 is released during H. pylori infection, thereby promoting gastric carcinogenesis. Our study further reveals that the aqueous extract of T. chebula can effectively inhibit the inflammatory responses driven by PTPN11 (SHP2), which highlights the therapeutic potential of targeting this protein in mucosal immunity.

ABL1, PTPN11/SHP2, and Ras constitute a crucial signaling transduction module that plays an indispensable role under both physiological and pathological conditions. Aberrant activation of this signaling axis is one of the core mechanisms driving the malignant phenotypes of cells in malignant tumors (e.g., leukemia) and infection-associated carcinogenesis (e.g., H. pylori-associated gastric cancer). ABL1 initiates the signaling cascade, SHP2 acts as a key transducer and amplifier, and Ras ultimately executes the pro-proliferative and pro-survival instructions [12–16].

An in-depth understanding of the network interactions among these three molecules not only unravels the intrinsic logic underlying disease initiation and progression but also provides a solid theoretical basis for developing combined targeted therapies against this signaling axis. Future studies should aim to explore the optimal strategies for disrupting the synergistic effects of this signaling axis in specific cancer contexts and translate this knowledge into effective clinical therapeutic regimens.

The present study still has several limitations: the differences between the animal model and human chronic infection may affect the extrapolation of conclusions; network pharmacology may omit certain components or targets; the interactions among various active components have not been elucidated; and the hepatotoxicity risk indicated by animal experiments requires further clarification [19]. Future research should conduct clinical studies to verify the efficacy and safety, employ multi-omics technologies to further unravel the underlying mechanisms, and isolate and optimize active components for the development of new compound preparations. Meanwhile, exploring the synergistic effects of Terminalia chebula Retz. with existing antibiotics is expected to provide new strategies for overcoming H. pylori resistance.

In conclusion, the anti-H. pylori activity of Terminalia chebula Retz. does not depend on a single component or mechanism, but rather reflects a comprehensive pharmacological mode of multi-component, multi-target, and multi-pathway synergistic actions. At the molecular level, its active

components, such as ellagic acid and quinine sulfate, can not only directly act on bacteria to inhibit their growth and proliferation, exerting a bacteriostatic effect, but also effectively suppress the excessive activation of the Ras signaling pathway and related inflammatory pathways through interacting with the PTPN11 (SHP2) target, thereby regulating the release of downstream inflammatory factors and alleviating the inflammatory damage of gastric mucosa. The synergistic operation of this dual mechanism of bacteriostasis and anti-inflammation highlights the potential advantage of Terminalia chebula Retz. in addressing both the symptoms and root causes during the intervention of H. pylori infection, and also provides a theoretical basis for further developing it as an adjuvant therapeutic agent.

## Declarations

# Author Contribution

Yangchenze Fan and Xuanru Kang drafted the main manuscript text.All authors reviewed the manuscript.

## References


1. Liu H, Shen J, Liu WB, et al. Protective effect and mechanism of aqueous extract of Terminalia chebula Retz. on rats with hyperuricemic nephropathy[J]. Pharmacology and Clinics of Chinese Materia Medica, 2024, 40(10): 56–64. DOI: 10.13412/j.cnki.zyyl.20240412.004.
2. Imai S, Ooki T, Murata-Kamiya N, et al. Helicobacter pylori CagA elicits BRCAness to induce genome instability that may underlie bacterial gastric carcinogenesis. Cell Host Microbe. 2021;29(6):941–958.e10. doi:10.1016/j.chom.2021.04.006
3. Kashyap D, Baral B, Jakhmola S, Singh AK, Jha HC. Helicobacter pylori and Epstein-Barr Virus Coinfection Stimulates Aggressiveness in Gastric Cancer through the Regulation of Gankyrin. mSphere. 2021;6(5):e0075121. doi: 10.1128/mSphere.00751-21. Epub 2021 Sep 29. PMID: 34585958; PMCID: PMC8550222.
4. Fei X, Chen S, Li L, Xu X, Wang H, Ke H, He C, Xie C, Wu X, Liu J, Xie Y, Lu N, Zhu Y, Li N. Helicobacter pylori infection promotes M1 macrophage polarization and gastric inflammation by activation of NLRP3 inflammasome via TNF/TNFR1 axis. Cell Commun Signal. 2025;23(1):6. doi: 10.1186/s12964-024-02017-7. PMID: 39762835; PMCID: PMC11705855.
5. Liu C, Meng XM, Nian YY, et al. In vitro bacteriostatic effect of Sino-Mongolian medicines on Helicobacter pylori[J]. Journal of Modern Integrated Traditional Chinese and Western Medicine, 2024, 33(16): 2244–2249.
6. Zhang M, Cui S, Mao B, Zhang Q, Zhao J, Zhang H, Tang X, Chen W. Ellagic acid and intestinal microflora metabolite urolithin A: A review on its sources, metabolic distribution, health benefits, and biotransformation. Crit Rev Food Sci Nutr. 2023;63(24):6900–6922. doi: 10.1080/10408398.2022.2036693. Epub 2022 Feb 10. PMID: 35142569.
7. Zhang XJ, He LJ, Lu Q, Li DY. [Pharmacological activity of Terminalia chebula]. Zhongguo Zhong Yao Za Zhi. 2016;41(4):619–623. Chinese. doi: 10.4268/cjcmm20160412. PMID: 28871682.
8. Ou L, Liu HR, Shi XY, Peng C, Zou YJ, Jia JW, Li H, Zhu ZX, Wang YH, Su BM, Lai YQ, Chen MY, Zhu WX, Feng Z, Zhang GM, Yao MC. Terminalia chebula Retz. aqueous extract inhibits the Helicobacter pylori-induced inflammatory response by regulating the inflammasome signaling and ER-stress pathway. J Ethnopharmacol. 2024;320:117428. doi: 10.1016/j.jep.2023.117428. Epub 2023 Nov 18. PMID: 37981121.
9. Liang XL, Hu HB, Jia AP, et al. Correlation study between gastric cancer, PTPN11 gene polymorphism and Helicobacter pylori infection[J]. Journal of Youjiang Medical University for Nationalities, 2011, 33(3): 261–263.
10. Wu WC, Xu LM, Lai YQ, et al. Relationship between Helicobacter pylori OipA and expression of p53 and ras proteins in gastric cancer tissues[J]. Journal of Practical Medicine, 2012, 28(13): 2156–2158.
11. Kazemi-Sefat GE, Keramatipour M, Vaezi M, et al. Integrated genomic sequencing in myeloid blast crisis chronic myeloid leukemia (MBC-CML), identified potentially important findings in the context of leukemogenesis model. Sci Rep. 2022;12(1):12816. Published 2022 Jul 27. doi:10.1038/s41598-022-17232-w
12. Craig VJ, Cogliatti SB, Rehrauer H, Wündisch T, Müller A. Epigenetic silencing of microRNA-203 dysregulates ABL1 expression and drives Helicobacter-associated gastric lymphomagenesis. Cancer Res. 2011;71(10):3616–3624. doi:10.1158/0008-5472.CAN-10-3907
13. Goto Y, Ando T, Yamamoto K, et al. Association between serum pepsinogens and polymorphismof PTPN11 encoding SHP-2 among Helicobacter pylori seropositive Japanese. Int J Cancer. 2006;118(1):203–208. doi:10.1002/ijc.21338
14. He C, Tu H, Sun L, Xu Q, Gong Y, Jing J, Dong N, Yuan Y. SNP interactions of Helicobacter pylori-related host genes PGC, PTPN11, IL1B, and TLR4 in susceptibility to gastric carcinogenesis. Oncotarget. 2015;6(22):19017–26. doi: 10.18632/oncotarget.4231. PMID: 26158864; PMCID: PMC4662472.
15. Kashyap D, Baral B, Jakhmola S, Singh AK, Jha HC. Helicobacter pylori and Epstein-Barr Virus Coinfection Stimulates Aggressiveness in Gastric Cancer through the Regulation of Gankyrin. mSphere. 2021;6(5):e0075121. doi: 10.1128/mSphere.00751-21. Epub 2021 Sep 29. PMID: 34585958; PMCID: PMC8550222.
16. Yang F. Study on Chemical Components and Toxic Mechanism of Hepatotoxic Extraction Fractions from Terminalia chebula Retz.[D]. Northeast Agricultural University, 2022. DOI: 10.27010/d.cnki.gdbnu.2022.000502.

# Figures

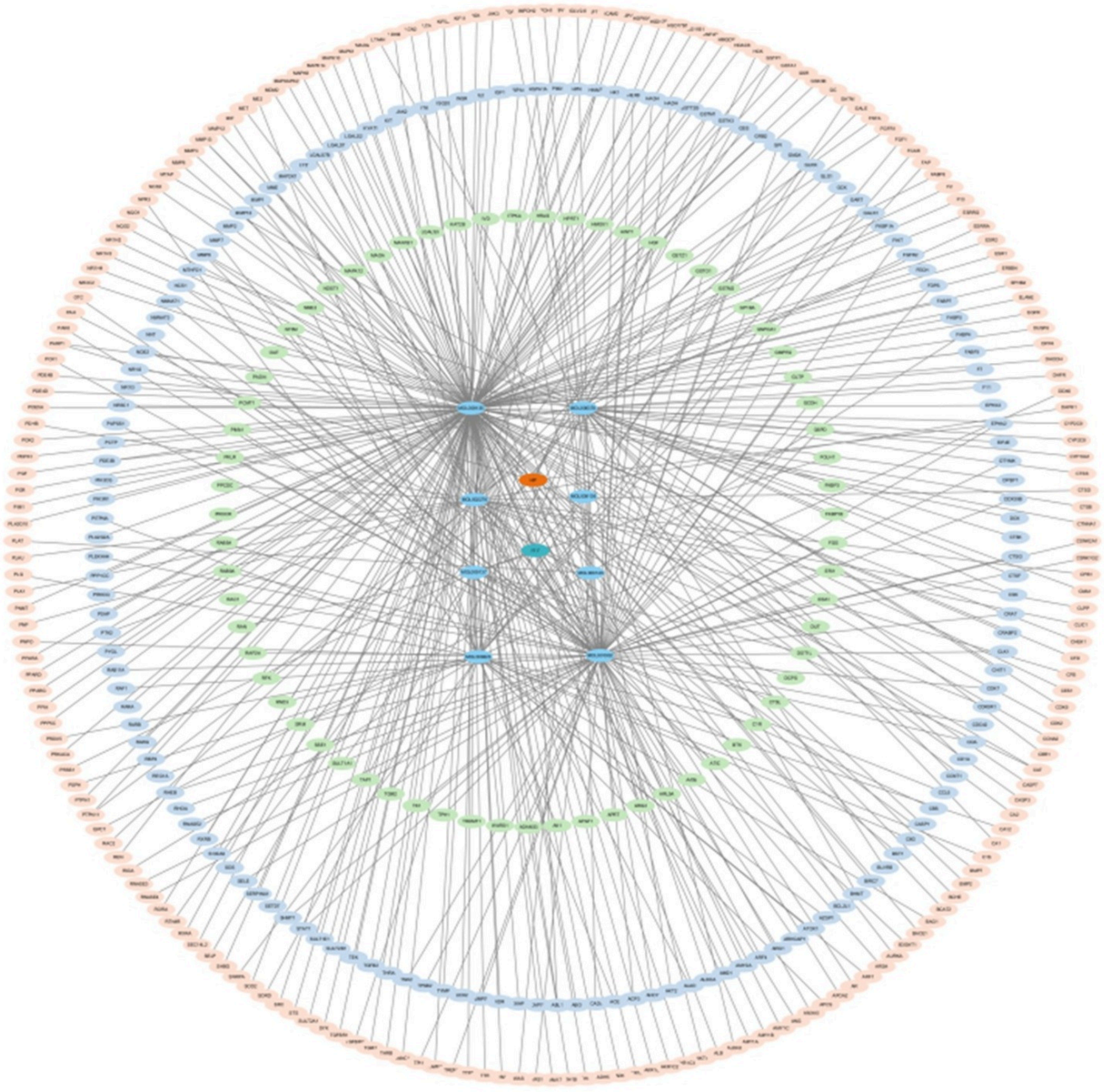

Figure 1

Active Component-Target Network Diagram

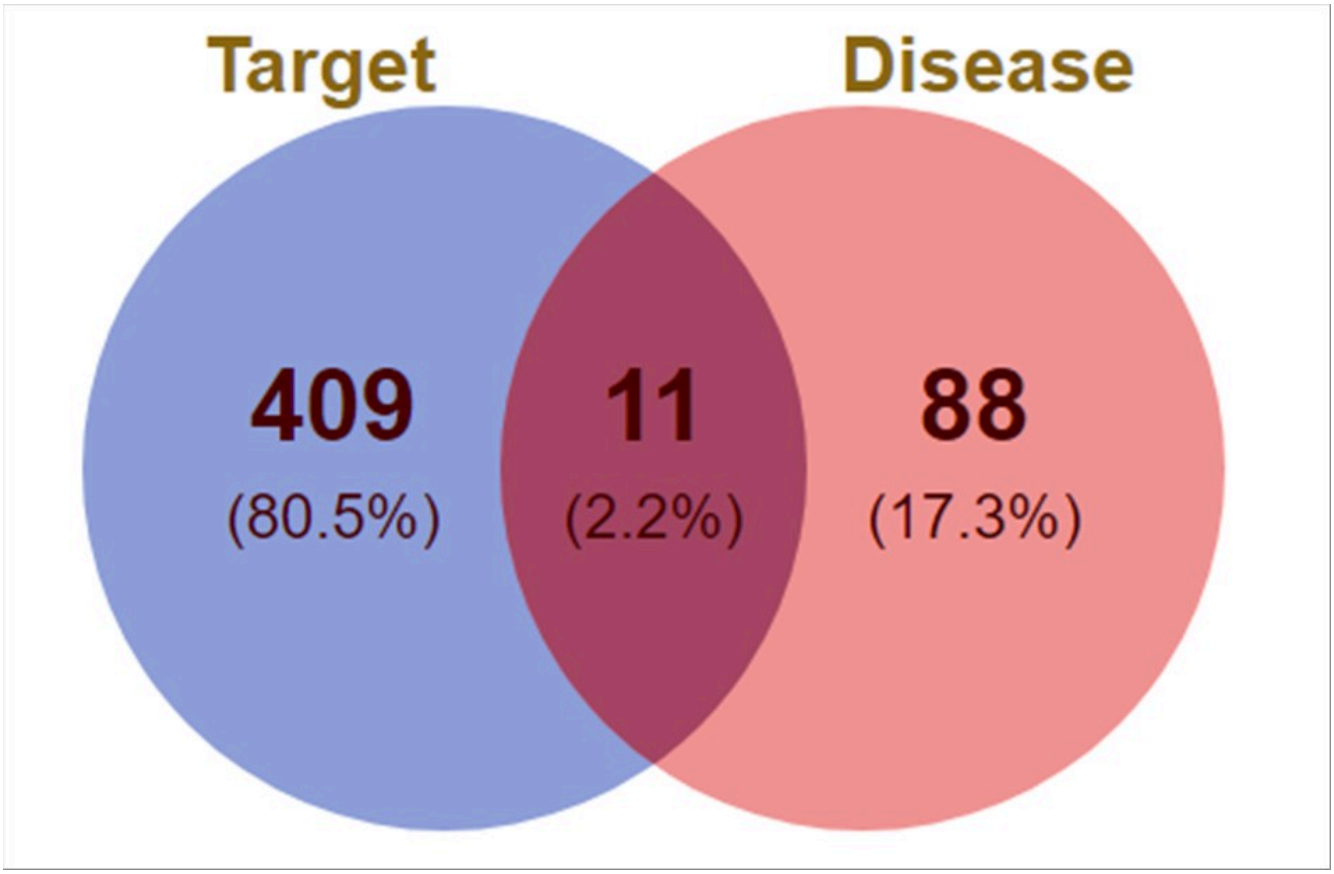


Figure 2

Venn Diagram of Targets of Active Components from Terminalia chebula Retz. and Pathogenic Targets of Helicobacter pylori

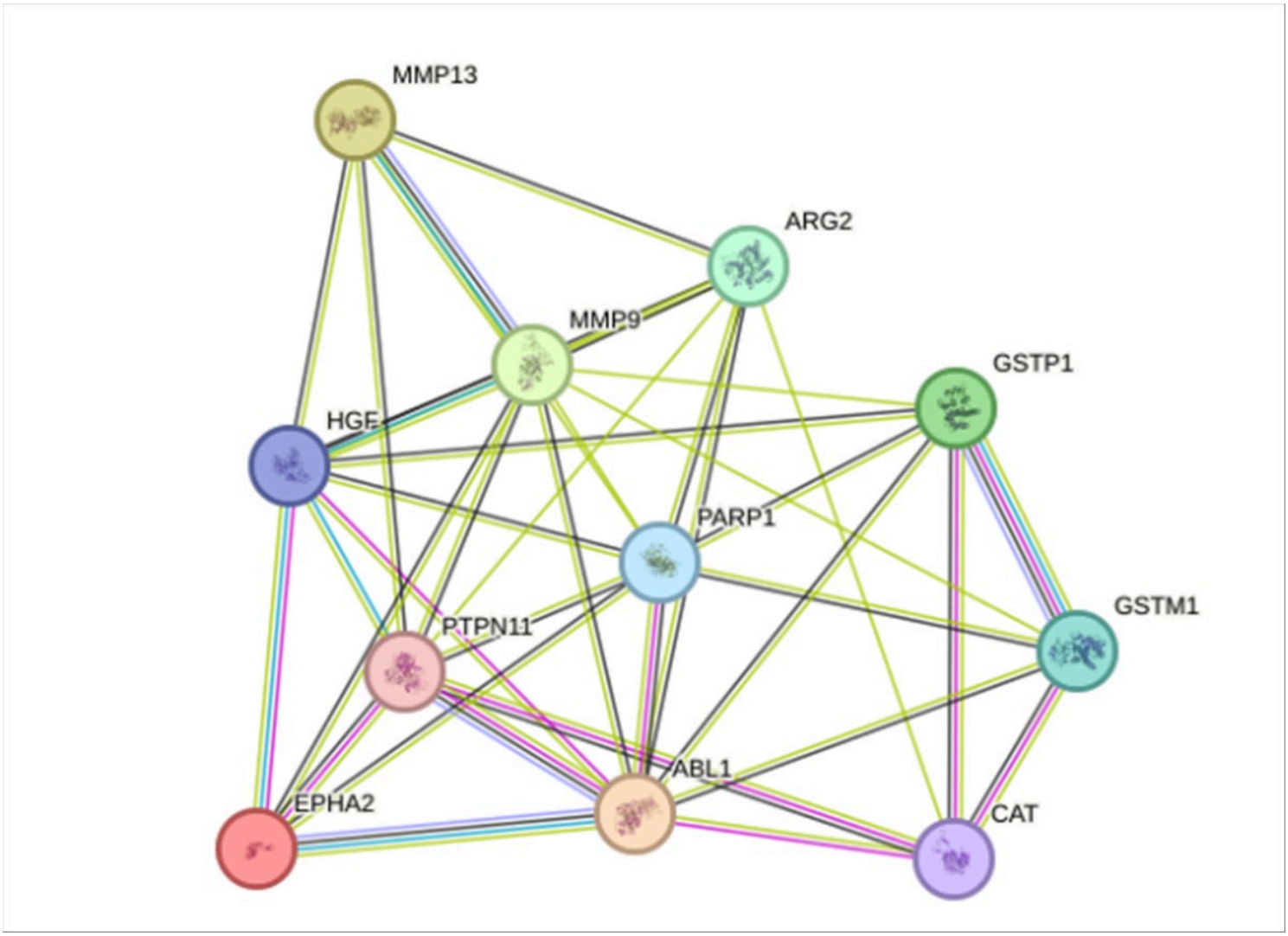


Figure 3

PPI Network Diagram of Interaction Targets between Terminalia chebula Retz. and Helicobacter pylori

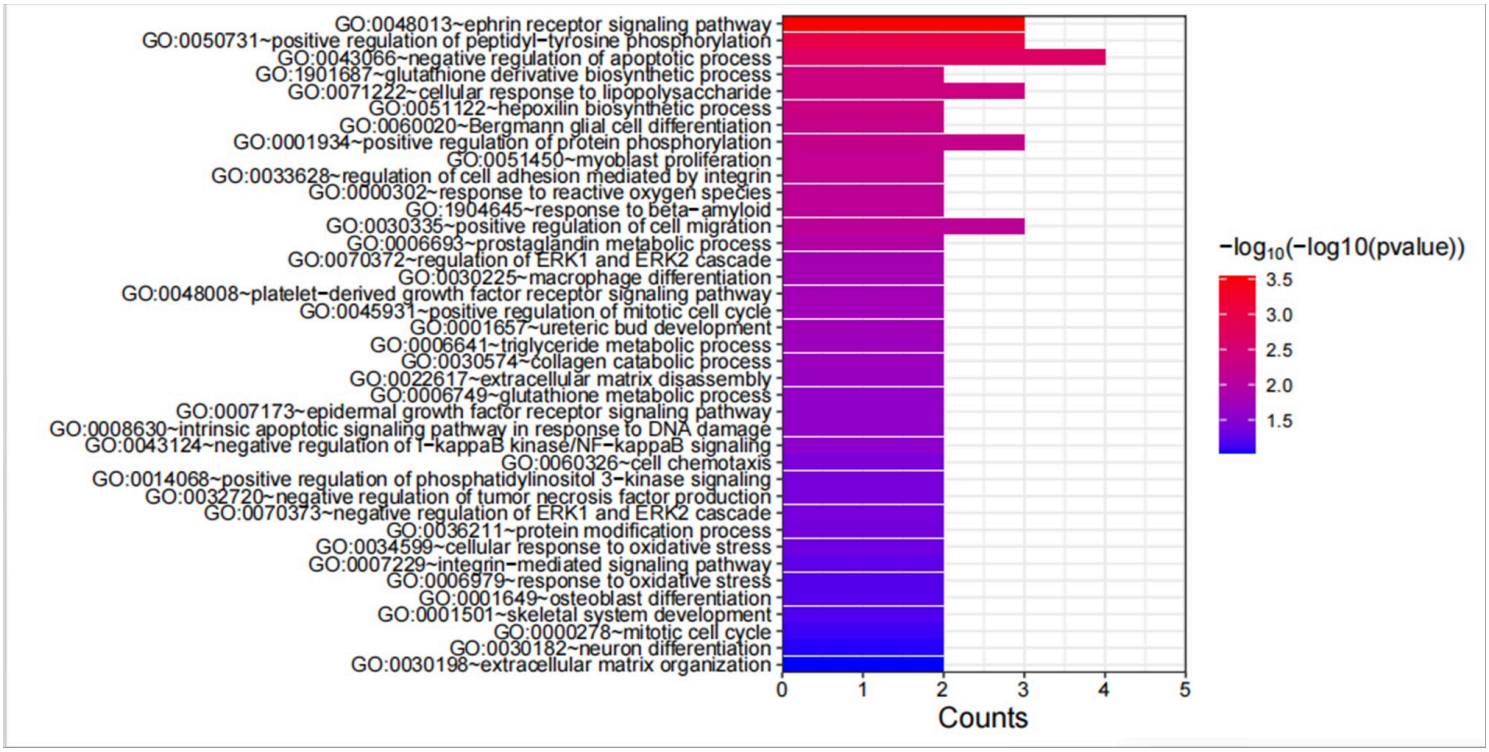


Figure 4

GO-BP Bar Chart

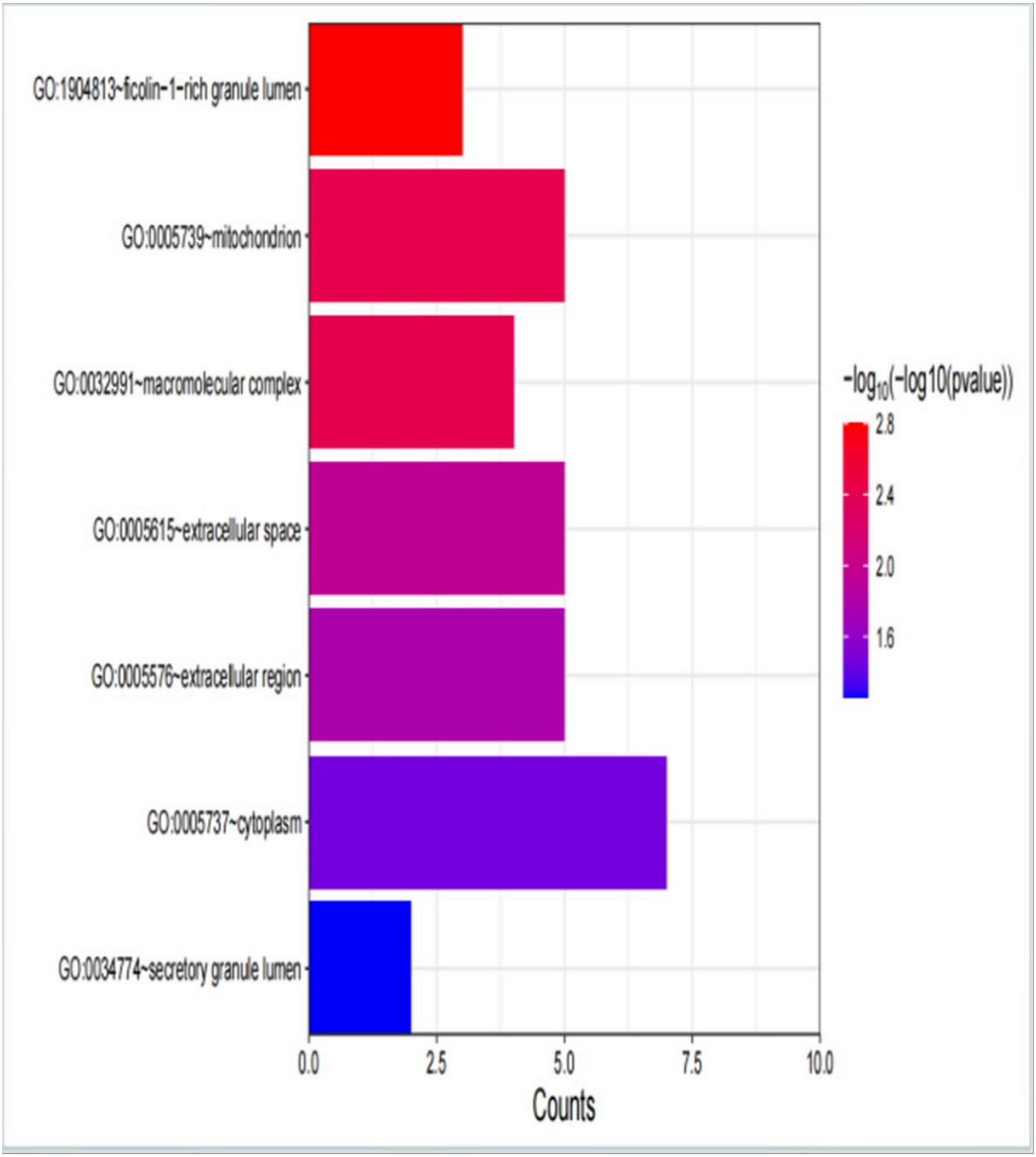


Figure 5

GO-CC Bar Chart

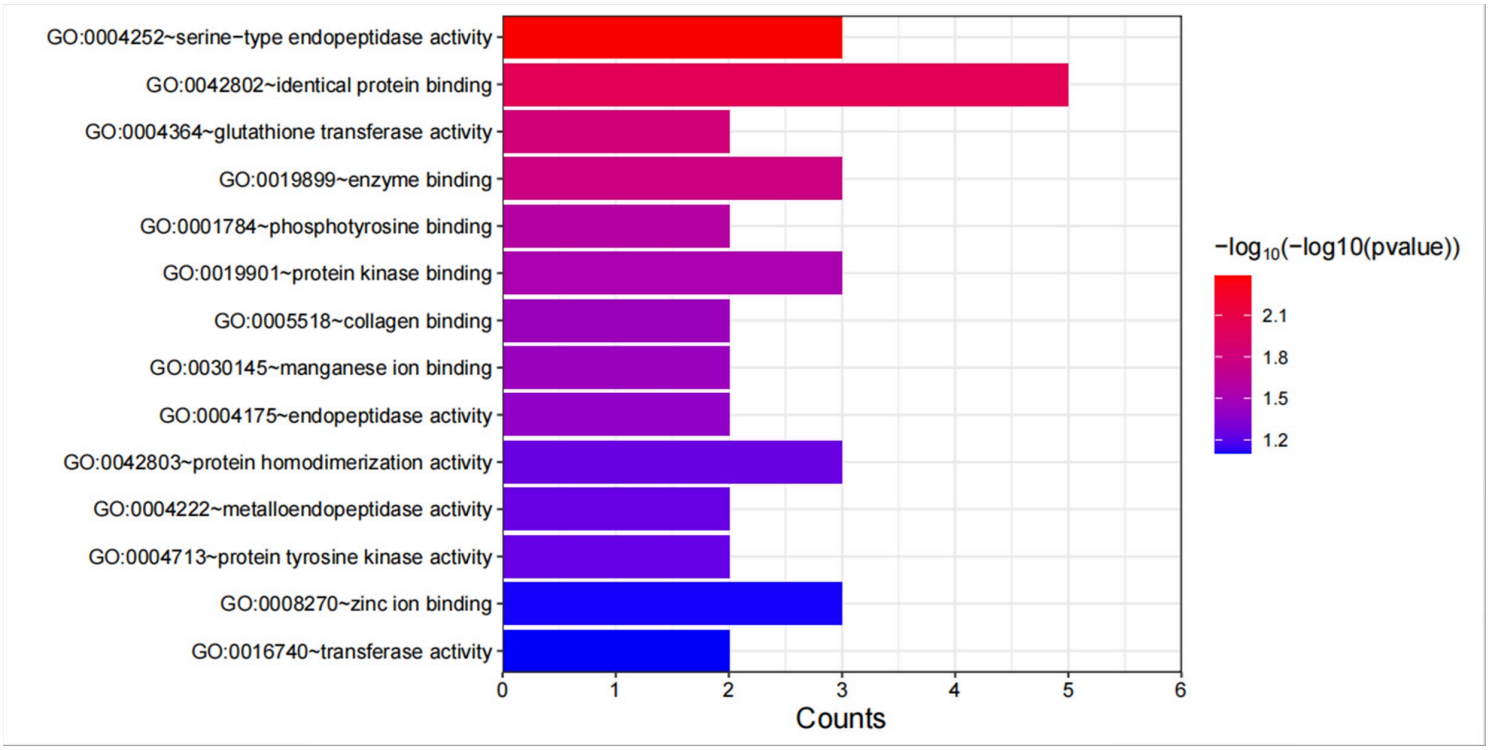


Figure 6

GO-MF Bar Chart

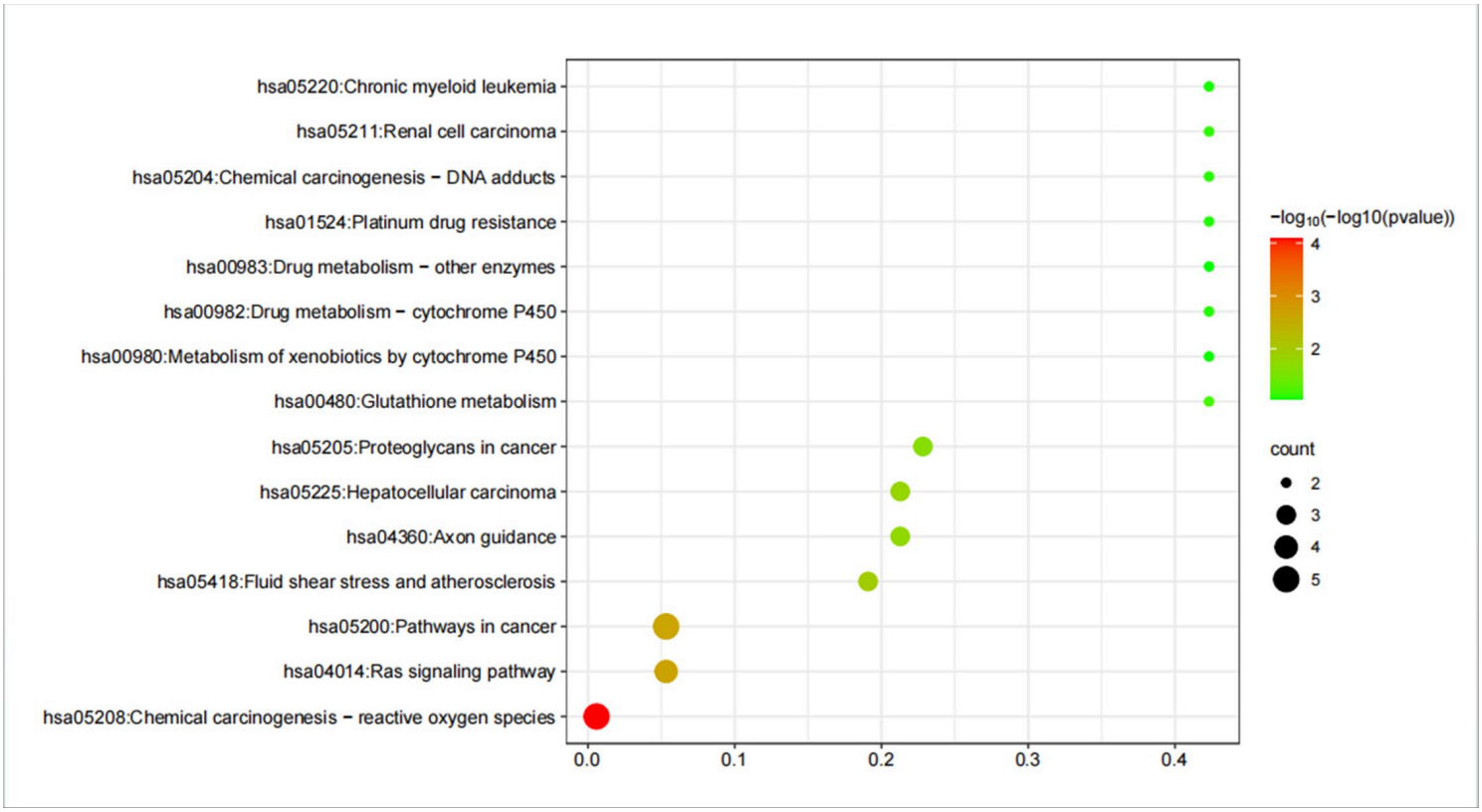


Figure 7

KEGG Bubble Chart

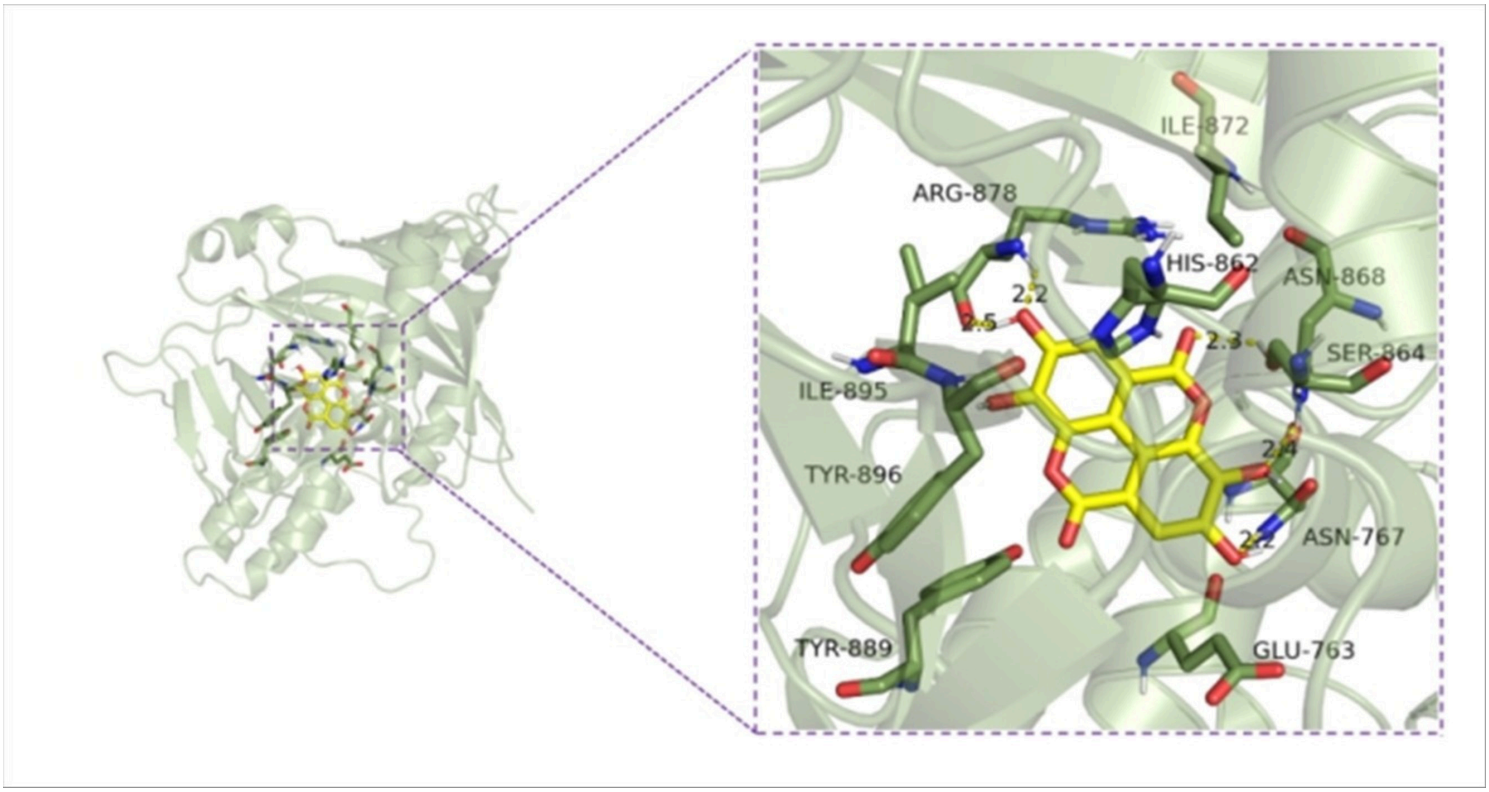


Figure 8

Optimal Docking Diagram of Key Targets Inhibiting Helicobacter pylori and Active Components (ellagic acid and PARP1)

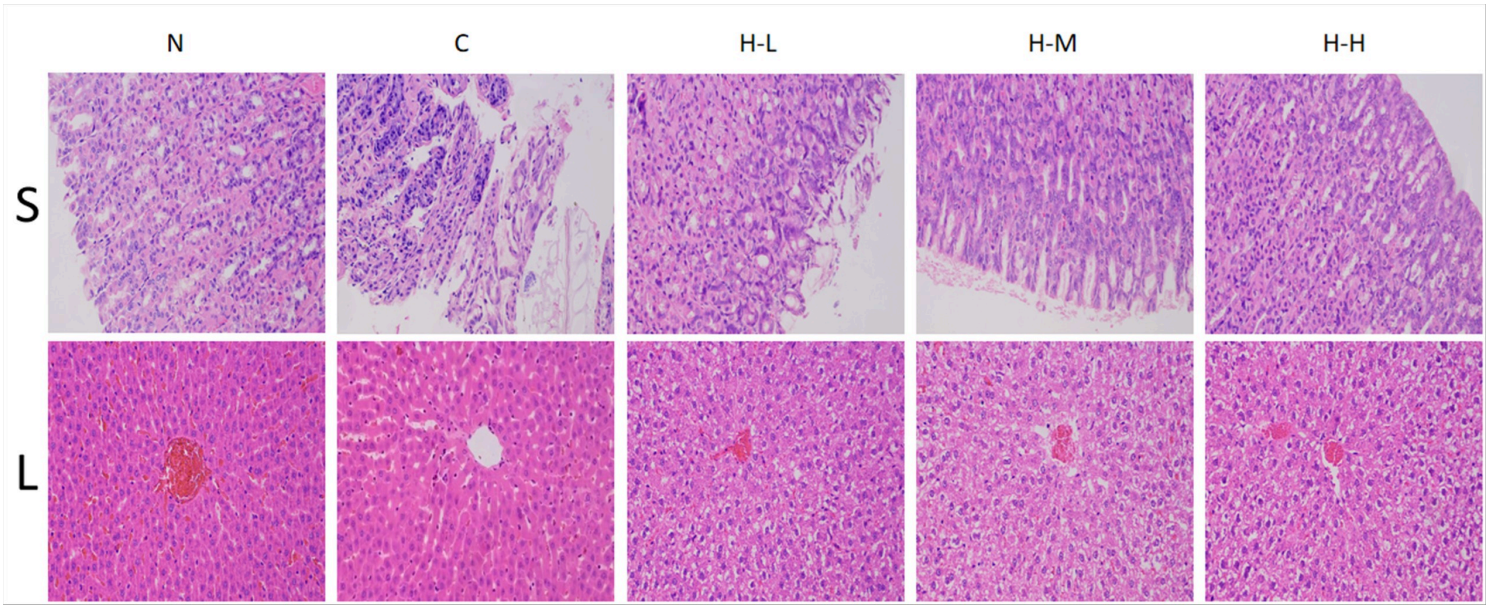


Figure 9

Note: N = Normal Group; C = H. pylori Infection Group; H-L = Terminalia chebula Low-Dose Group; H-M = Terminalia chebula Medium-Dose Group

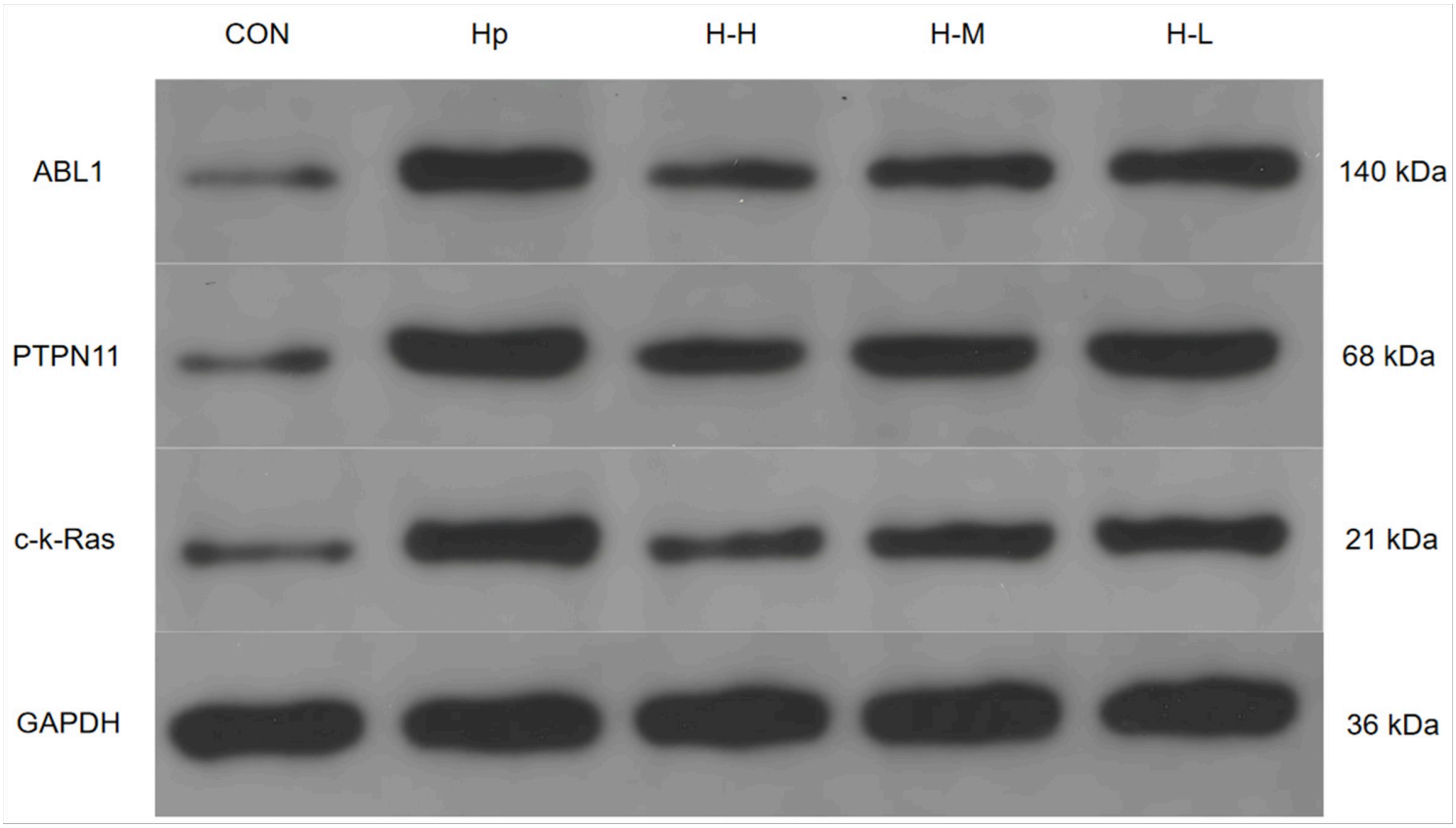


Figure 10

WB Band Image

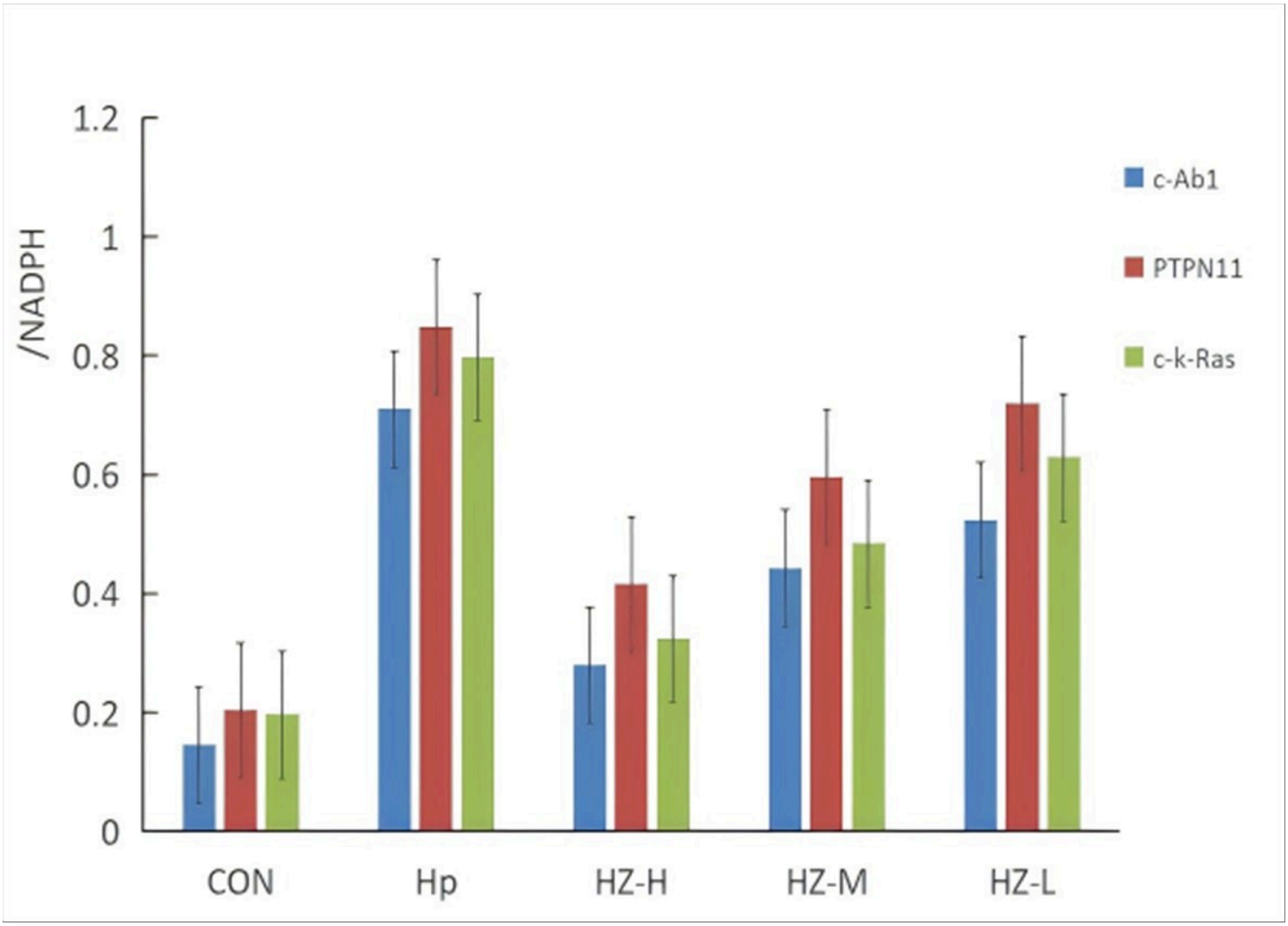


**Figure 11**

**Horizontal Bar Chart**

Note: CON = Control Group; Hp = H. pylori Infection Group; H-L = Terminalia chebula Retz. Low-Dose Group; H-M = Terminalia chebula Retz. Medium-Dose Group; H-H = Terminalia chebula Retz. High-Dose Group